Raman Tweezers for small microplastics and nano-plastics identification in seawater.

Raymond Gillibert,[1] Gireeshkumar Balakrishnan,[2] Quentin Deshoules,[3] Morgan Tardivel,[3] Alessandro Magazzù,[4] Maria Grazia Donato,[1] Onofrio M. Maragò,[1] Marc Lamy de La Chapelle,[2] Florent Colas,[3] Fabienne Lagarde,[2] Pietro G. Gucciardi[1,]*

[1] CNR – IPCF, Istituto per i Processi Chimico-Fisici, Viale F. Stagno D'Alcontres 27, I- 98158 Messina, Italy

[2] Institut des Molécules et Matériaux du Mans, UMR 6283 CNRS, Le Mans Université, Le Mans, France

[3] Ifremer LDCM, Centre Bretagne, CS 10070, 29280 Plouzané, France

[4] Department of Physics, University of Gothenburg, 41296 Gothenburg, Sweden

Keywords: Microplastics, Nanoplastics, Optical Tweezers, Raman Spectroscopy.

ABSTRACT

Our understanding of the fate and distribution of micro- and nano- plastics in the marine environment is limited by the intrinsic difficulties of the techniques currently used for the detection, quantification and chemical identification of small particles in liquid (light scattering, vibrational spectroscopies, optical and electron microscopies). Here we introduce Raman Tweezers (RTs), namely optical tweezers combined with Raman spectroscopy, as an analytical tool for the study of micro- and nano-plastics in sea water. We show optical trapping and chemical identification of sub-20 μm plastics, down to the 50 nm range. Analysis at the single particle level allows us to unambiguously discriminate plastics from organic matter and mineral sediments, overcoming the capacities of standard Raman spectroscopy in liquid, intrinsically limited to ensemble measurements. Being a microscopy technique, RTs also permits to assess the size and shapes of particles (beads, fragments, fibres), with spatial resolution only limited by diffraction. Applications are shown on both model particles and naturally aged environmental samples, made of common plastic pollutants, including polyethylene, polypropylene, nylon and polystyrene, also in presence of a thin eco-corona. Coupled to suitable extraction and concentration protocols, RTs have the potential to strongly impact future research on micro and nanoplastics environmental pollution, and enable the understanding of the fragmentation processes on a multi-scale level of aged polymers.

INTRODUCTION

Microplastics[1,2] and nanoplastics pollution[3] is currently perceived as the last frontier in environmental research.[4,5,6,7,8,9] The transfer of very small plastics through the trophic chain[10,11,12] is a potential source of contamination at all the trophic levels and the potential impacts on the human health have raised concerns.[13,14] Surveys are, however, limited to particles > 20 µm (e.g. [15,16,17,18]), with very few reports addressing the sub-20 µm fraction.[19,20,21] Data on nanoplastics[22] (particles smaller than 1 µm) are even more scarce. The generation of nanoplastics has been demonstrated by photodegradation,[23,24] or biodegradation[25] of microplastics. Their presence in the North Atlantic subtropical gyre has recently been suggested.[3] The ingestion of plastic nanocolloids has been demonstrated in oysters.[26,27] The quest for sub-20 µm microplastics has become particularly relevant in view of recent reports showing that the quantity of plastics detected in the oceans is orders of magnitude smaller than expected, and suggesting that the undetected micrometric and nanometric fraction, derived from fragmentation of millimetre scale particles, could account for this deficiency.[15,16]

Well assessed protocols have been developed for the analysis of microplastics in the 5 mm – 20 µm range.[28,29] These include visual inspection / stiffness test (down to 500 µm),[28,30,31] FTIR/microFTIR,[12,17, 32,33,34] Raman/micro-Raman,[19,33,35,36] Pyrolysis Gas Chromatography–Mass Spectroscopy (down to 100 µm),[37,38,39,40] Transmission/Scanning Electron Microscopy (TEM/SEM),[19,38] Fluorescence Microscopy.[16,21,41] It is a shared opinion, instead, that methods to characterize the chemical nature of the smallest micro and nanoplastics, especially in water environment, are still to be invented.[22,30,42,43,44] The techniques used so far, in fact, include

TEM/SEM,[9,22,23] fluorescence microscopy,[26] Nanoparticles Tracking Analysis[24] and Dynamic Light Scattering,[22,23] none of which is capable to provide chemical information.

Among the "classical" analytical techniques microRaman can, indeed, be used to probe nanosized materials.[45] Although the spatial resolution is limited by diffraction (~250 nm), sensitivity reaches the single nanostructure level. Few nm diameter carbon nanotubes,[46] one-atom thick graphene flakes[47] and plastic particles of few tens of nanometers[48] are easily detectable. Infrared – Atomic Force Microscopy (AFM-IR),[49] Near-Field Raman Microscopy, Tip-Enhanced Raman Spectroscopy (TERS),[50] and Nano-FTIR[51] combine chemical sensitivity with nanoscale resolution.[52,53,54] Such tools are, however, very expensive, require bulky setups and none of them is capable to analyse particles in liquid dispersions.

Optical Tweezers (OT) exploit the tiny forces that light exerts on matter[55,56] to trap and manipulate micro and nanoparticles dispersed in liquid.[57,58] When coupled to Raman spectrometers, OT enable chemical analysis of the trapped particles. The so-called Raman Tweezers (RT)[59,60] find applications in several fields[61] including cells sorting,[62] virology,[63] nanomaterials analysis,[64,65] and high sensitivity molecular detection.[66,67,68,69] First demonstrations of the potentialities of OT/RT in the field of nanoplastics (although the name was far from being invented) were shown by Ashkin et al. in 1986,[56] who stably trapped 25 nm PS spheres in water, and by Ajito *et al.* in 2002, [70] who showed Raman spectra of optically trapped 40 nm PS spheres. To our best knowledge, no applications of RTs in the study of nanoplastics pollution have been published so far.

Here we propose the use of RTs to trap and chemically identify a broad range of small micro- and nanoplastics in both distilled and seawater, showing unambiguous discrimination between different plastics and microparticles coming from marine sediments and organic matter. Results are

shown on commercial, artificially produced and naturally aged fragmented particles (50 nm – 20 µm diameter) made of Polypropylene (PP), Polystyrene (PS), Polyethylene(PE), Polyamide-6 (PA6), Poly-Vinyl-Alcohol (PVA), Poly-methyl-methacrylate (PMMA) and Polyethylene-terephthalate (PET).

THEORETICAL BASIS

Definitions. Plastics in seawater undergo fragmentation into debris of smaller size (Figure 1a).[71] The European Water Framework (EWF) directive[72] defines microplastics particles < 5 mm. The lower size bound of microplastics is arbitrarily set by the different authors. Consensus on the definition of nanoplastics is still missing [Note S1, Supporting Information (SI)]. In this article we use the EWF definition for the term microplastics and the term nanoplastics for particles smaller than 1 µm in at least two dimensions, no matter whether they are produced intentionally (primary sources[73,74,75,76]) or come from fragmentation of larger objects (secondary sources).[22] We refer to microplastics smaller than 20µm as "the sub-20 µm fraction." We call "large nanoplastics" those between 1 µm and 100 nm and "small nanoplastics" the ones smaller than 100 nm (Figure 1b).

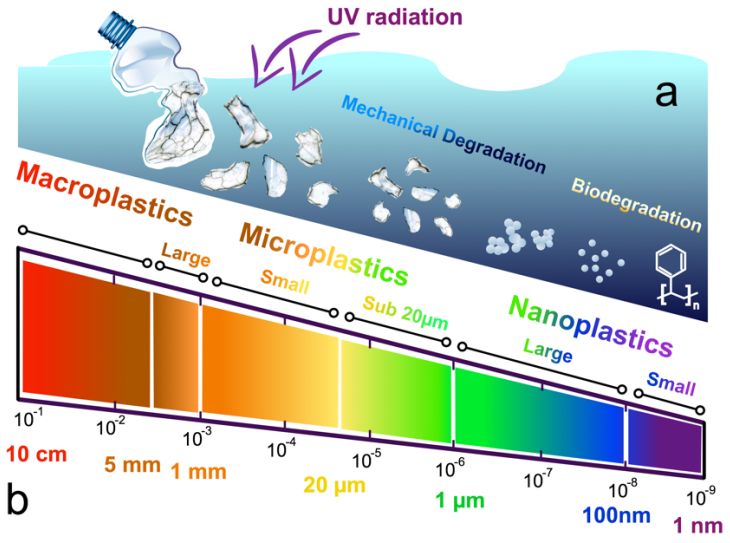

Figure 1: Degradation flow and size-based definition of plastics.

Optical Forces are due to the momentum exchange between light and particles during the scattering interaction,[57] arising when tightly focusing laser beams. They confine particles in an optical potential well, giving rise to the so-called optical trapping. Different approximation models can be used to calculate optical forces.[61] The size parameter $x = k_m a$ defines the range of validity of each approximation, where $k_m = 2\pi n_m/\lambda$, is the light wavenumber in the medium surrounding the particle, n_m the medium refractive index ($n_m = 1.33$ for water), a is the particle radius (10 nm – 10 µm for the sub-20 µm plastics fraction) and λ is the laser wavelength in vacuum (400 – 1100 nm for standard applications).

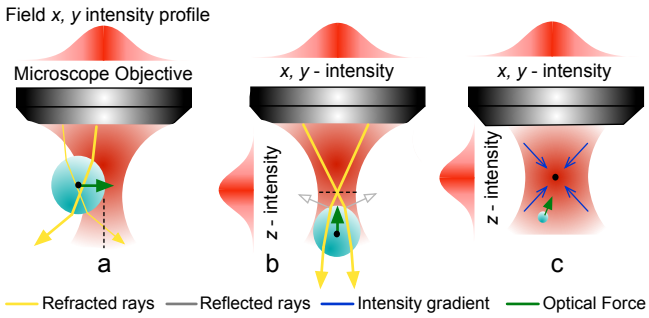

Figure 2. Diagram illustrating the principle of OT in to the ray optics regime (a, b) valid for microplastics down to several microns in size, and in the Rayleigh regime (c) valid for the nanoplastics.

For particles much bigger than the wavelength ($x \gg 1$), i.e. for microplastics down to sub-20 µm fraction, the ray optics approximation (ROA) is used.[77] The optical field is split in a collection of light rays, each carrying a portion of the total power and linear momentum. When each ray

impinges on the particle, it will be partly refracted and partly reflected by the surface, according to Snell's law (yellow and grey lines in Figure 2a,b). The total interaction force is the sum of the components generated by the reflection and refraction of each ray (Note S2, SI). When the particle is displaced laterally with respect to the optical axis (Figure 2a), a net transverse force arises (green arrow), proportional to the field intensity gradient (transverse gradient force), that pulls back the particle towards the optical axis, whenever the particle's refractive index, n_{p}, is larger than the medium one n_{m}, i.e. $n_{\mathrm{p}} > n_{\mathrm{m}}$. Figure S1(a), SI, shows the transversal gradient force acting on a 10 μm diameter PE bead as a function of the position ($x = 0$ is the optical axis). For small displacements, the force is proportional to the displacement (Hook's law) and tends to bring the particle to the equilibrium position ($x = 0$), independently from the objective's numerical aperture, *NA* ($NA = n_{\mathrm{m}} \sin\theta$, where n_{m} is the refractive index of the medium and θ is objective's aperture angle). When the particle is displaced axially below the laser focus (Figure 2b), the overall direction of the laser propagation is not changed, but its divergence is. The transmitted rays are refracted in a way that they are more convergent upon leaving the particle (Figure 2b, yellow lines). This slight change of the rays' orientation causes a restoring force acting upwards (green arrow) and proportional to the field intensity gradient (longitudinal gradient force). If the particle is located above the focus the restoring force will point downwards. The gradient force ($\vec{F}_{\mathrm{grad}}$), whether transverse or longitudinal, yields the trapping of the particle in the laser focus. A second optical force, the scattering force ($\vec{F}_{\mathrm{scat}}$), due to the radiation pressure induced by the recoil of the reflected rays (Figure 2b, grey lines) tends, instead, to destabilize the optical trap, pushing the particle along the beam propagation direction. Stable 3D trapping (Movie S1, SI) requires that the longitudinal gradient force overcomes the scattering force. In the ROA this occurs when the objective's *NA* is large enough to create a field gradient capable to counterbalance the effect of the radiation pressure.

Figure S1(b), SI, shows this effect for a 10 µm PE particle. For *NA* > 1.0 (red, magenta) the net longitudinal force and the trap stiffness are strong enough to provide stable trapping. For *NA* = 0.3 the force (green) is almost flat around $z = 0$ and the trap becomes unstable. *NA* = 0.6 (blue) is an intermediate situation in which weak trapping is expected. For non-spherical particles, shape-dependent optical torques lead to alignment or rotation effects (Movie S2, SI).[61]

For particles much smaller than the laser wavelength ($x \ll 1$), e.g. small nanoplastics, the dipole approximation is adopted (Note S2, SI). The particle is modelled as a point-like dipole $\vec{p}$ induced by the incident field $\vec{E}$. The (oscillating) induced dipole interacts with the (oscillating) incident electromagnetic field, leading to a force whose time-averaged expression is:[61]

$$\langle \vec{F} \rangle = \underbrace{\frac{1}{4}\,\mathrm{Re}(\alpha)\,\vec{\nabla}\left|\vec{E}(\vec{r})\right|^2}_{\text{Gradient Force}} + \underbrace{\frac{n_\mathrm{m}}{2c}\,\sigma_\mathrm{ext}\,\mathrm{Re}\left(\vec{E}\times\vec{H}^*\right)}_{\text{Radiation pressure}} + \underbrace{\frac{c\,n_\mathrm{m}\,\varepsilon_\mathrm{m}}{4i\omega}\,\sigma_\mathrm{ext}\,\vec{\nabla}\times\left(\vec{E}\times\vec{E}^*\right)}_{\text{Spin-curl Force}} \qquad (1)$$

Here $\mathrm{Re}(\alpha)$ is the real part of the particle's polarizability, $\left|\vec{E}(\vec{r})\right|^2$ the intensity spatial profile of field, $\vec{H}^*$ is the complex conjugate of the magnetic field, ω the angular frequency, σ_ext the extinction cross section of the particle, ε_m the dielectric constant of the medium. The first term is the gradient force. Plastics, featuring positive values of $\mathrm{Re}(\alpha)$, will be attracted and trapped in the maximum of the laser intensity, i.e. the focus of the objective (Figure 2c). The second term is the scattering force. It accounts for the radiation pressure and pushes the particle outside the trap. The third term is a spin dependent force, negligible in most of the cases. Figures S1(c, d), SI, shows the transverse and longitudinal forces acting on a 90 nm PS particle at 830 nm excited through objectives of different *NA*. Again, a restoring force attracts the particle in the laser focus for small displacements from the equilibrium. Objectives with numerical apertures $NA \geq 1$ are necessary to achieve stable trapping in the longitudinal direction (the force is flat for NA ≤ 0.6). For PS spheres at 830 nm, the dipole approximation provides accurate predictions for particles < 100 nm,[61] namely

for all small nanoplastics, while the ROA can be safely applied for particles > 1 μm, that is for all microplastics, including the sub-20 μm fraction.

In the intermediate regime, typical of large nanoplastics, where the particle size is comparable with the wavelength ($x \sim 1$) or for highly non-spherical or non-homogeneous particles, a complete wave-optical modelling is needed.[57]

Optical trapping of nanoplastics. Raman spectroscopy of micro- and nanoplastics requires measurement times up to few minutes, during which the particle must be stably trapped. For micron scale particles this is achieved when the refractive index of the particle is larger than the medium and when the objective's *NA* is large enough. For polymers n_{p} varies in the 1.3 – 1.7 range.[78] Values relative to the most common plastics (Table S1, SI) are indeed larger than water (n_{w} = 1.33). Therefore, using an objective with *NA*=1.3 (100X, oil immersion), stable trapping is always expected. The same does not necessary hold for nanoplastics, for which the laser power becomes important. For small enough particles, in fact, the Brownian motion can destabilize the optical trap. Having a gradient force stronger than the radiation pressure is a condition no more sufficient for stable trapping. In addition, the depth of the trapping potential well must be sufficient to overcome the thermal kinetic energy of the particle. This requires (Note S3, SI) that the laser power exceeds a certain threshold value, proportional to the square of the laser wavelength ($P_{\mathrm{thr}} \sim \lambda^2$) and to the inverse of the particle's volume ($P_{\mathrm{thr}} \sim a^{-3}$). More intense lasers are, therefore, needed to trap smaller particles or whenever we use longer wavelengths (e.g. in the NIR). Figure S2(a), SI, shows that powers of 1 – 50 mW are sufficient for stable 3D trapping of PS particles with diameter down to 100 nm (small nanoplastics limit), while several hundreds of mW are needed to access the sub-

50 nm regime. Figure S2(b), SI, shows that powers of several tens of mW are needed for stable 3D trapping of nanoplastics (100 nm) made of all common plastics materials.

EXPERIMENTAL SECTION

Raman Tweezers setup. A RT is an inverted microscope provided with a high *NA* objective, coupled to a Raman spectrometer. The high *NA* ensures the large intensity gradient necessary for trapping and, at the same time, the power density needed to maximize the Raman signal. The setup used for our experiments is a homemade single beam RT (Figure 3) in which the same laser is used for both Raman excitation and trapping.

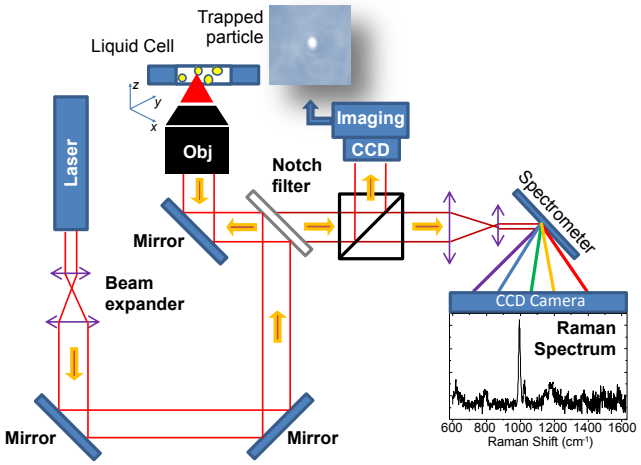

Figure 3. Sketch of the single beam Raman Tweezers setup used in our experiments.

It is coupled to several laser sources, among which a He-Ne (633 nm, P = 11 mW on sample) and a diode (785 nm, P = 21 mW on sample). The beam is expanded and sent to a notch filter that reflects it towards the objective (100X, oil immersion objective, NA 1.3, WD 200 µm). Light is focussed onto the particle's located in a glass microchamber mounted on a piezoelectric table for positioning purposes. The backscattered light (Rayleigh + Raman) is filtered by the same notch filter to remove most of the Rayleigh scattering (OD = 7). A CCD camera is used for imaging

trapped particles. A monochromator with a 1200 groves/mm grating and a Peltier-cooled silicon CCD camera (1024×256 pixels, spectral resolution at 633 nm is ~ 8 cm^{-1}) is used for detection. For analysis, 10 µL of particles solution is cast between a flat microscope slide and a soda-lime coverslip, forming a 25 µm thick microchamber. The drop is let to spread on the coverslip surface and sealed with nail polish. microchamber. The drop is let to spread on the coverslip surface and sealed with nail polish. Thanks to the inverted geometry of the setup, particles denser than water that precipitate at the bottom of the microcell are visible and can still be analyzed. As well, particles less dense than water will settle at the top of the microcell and, thanks to the small thickness (25 µm) of the microcell, will be still in the field of view and analysis of the high NA objective.

PS beads with diameters of 50, 90, 500, 1000 and 2000 nm in distilled water are purchased from SERVA (90 nm) and Polysciences (50, 500, 1000, 2000 nm). Nominal particles densities are 3.64×10^{14} particles/mL, 3.64×10^{11} particles/mL, 4.55×10^{10} particles/mL and 5.68×10^{9} particles/mL for the 50, 500, 1000, 2000 nm samples. For the 90 nm plastics, the producer only provides information on the PS volume fraction in the dispersion (10%). Particles are diluted up to $1:10^7$ v/v in in both distilled water and seawater sampled from the Mediterranean Sea, in Torre Faro (Italy). Dilution allows us to have a few particles visible in the field of view of the microscope ($50\times40\times25$ μm^3), and eases the process of localization and trapping. Freely floating individual particles of 90 and 50 nm diameter are not identifiable under our microscope, differently from aggregates which can be localized and trapped.

PMMA beads of 300 nm diameter are purchased from Polysciences. The producer provides information on the solid volume fraction in the dispersion (2.5%). Particles are diluted in seawater with 100 µL of diluted 1:20 v/v surfactant to avoid aggregation, in order to have a few particles

visible in the field of view. Individual particles are easily distinguished from dimers and oligomers under the microscope.

PP microparticles have been kindly provided by Two H Chem ltd. (Propolder FPP4010). They come in fine particle powder form with a size distribution nominally centered around 11µm and standard deviation of 3.5 µm. The powder is first dispersed in distilled water (5 mg in 5 mL). To avoid aggregation, we add 100 µL of surfactant diluted 1:20 v/v in distilled water. For experiments the solution is further diluted 1:100 v/v in distilled or seawater.

Thermoplastic polyamide-6 particles have been produced by artificial ageing at IFREMER. Polymer sheets 200 µm thick are placed in stainless steel vessels filled with pure water. They are placed in a ventilated oven at 140 °C for 14 days. The internal pressure is set to 15 bars. The resulting solution is used "as prepared" or diluted 1:10 v/v in seawater.

PE particles with diameter between 400 nm and 1.6 µm have been prepared at Le Mans University using toluene-in-water emulsions after total dissolution of PE in the toluene phase.[79] Particles feature a concentration smaller than 0.2% (w/w) and are covered with a biosurfactant derived from algae in order to improve stability. The two samples analysed are prepared dispersed in ultrapure water and after addition of sea salt to reach the typical concentration of seawater (35 g/L).

PVC, PET and PMMA particles have been artificially produced by rubbing against a grinding wet stone for sharpening knives. We start from cm-scale plastic fragments extracted from a credit card (PVC), a plastic bottle (PET) and a plastic cup (PMMA). The plastic is rubbed against the stone and then the stone is repeatedly rinsed with distilled water. The process is repeated three times. Surfactant is added for experiments in seawater.

Marine sediments have been extracted from below the water level of the Torre Faro (Italy) sea-shore, around the high-tide line, and put in an 8ml vial with sea water. 100 µL of surfactant is added and the sample is shaken for 10 min to ensure that most sediments get in suspension. Prior to analysis, the sample is decanted for 1 min in order to let sand and other heavy sediments deposit. The supernatant is pipetted and directly put in the fluidic cell for RT analysis.

Naturally aged PE microparticles have been obtained from a bottle cap found along the shores of Torre Faro, which had visibly undergone long exposition to solar radiation and subject to weathering. Microplastic particles have been produced by breaking the cap in seawater, similarly to what happens when a plastic bottle is accidentally stepped on. Samples are collected in a vial and shaken, prior to extracting the supernatant used for analysis. In air, 0.1 mg of sub-mm fragments is released during each fragmentation event on average. We expect, therefore, that the total plastic dispersed in the seawater sample is of the order of some hundreds of µg/mL.

Naturally aged PP microparticles have been obtained from a paint bucket found along the shores of Torre Faro (Messina, Italy). The bucket looked aged and brittle, suggesting long exposure to weathering. Residual paint was present on the interior walls and it contained clam shells. Very little mechanical pressure was required to fragment the bucket walls into a large number of millimeter and sub-millimeter particles. The analysed samples have been produced by fragmenting parts of the bucket directly in seawater in a vial. After shaking, the supernatant has been pipetted and used for analysis. In air, circa 1 mg of sub-mm fragments is released during each fragmentation event on average. We expect, therefore, that the total plastic analysed in seawater is of the order of some mg/mL.

RESULTS AND DISCUSSION.

Experiments are carried out with the aim of (i) demonstrating that micro and nanoplastics made of different materials, shapes and sizes can be easily trapped and quickly analysed by RT in distilled and in sea water, (ii) showing that the Raman fingerprints of different plastics present in the same dispersion can be easily discriminated; (iii) showing that the plastics can be unambiguously distinguished from optically trapped sediments microparticles; (iv) provide a demonstration of RT analysis on two naturally aged, brittle samples found in the environment; (v) determining the best excitation wavelength in terms of ease of trapping, maximum signal, minimum acquisition time, minimum background. A database of the Raman fingerprints of different plastics has been preliminarily acquired using the RT setup, for reference purposes, on cm-scale fragments in dry conditions. Spectra, modes assignment and discussion are reported in SI (Figure S3, Note S4, Tables S2 – S8).

Detection and identification of micro- and nanoplastics in distilled water. Diluted solutions of PS spheres have been analysed at 785 nm (2 μm to 90 nm diameter) and on a larger dimensions range at 633 nm (5 μm to 50 nm diameter), in order to compare the trapping potentialities and signal levels. Pictures of the trapped particles are shown in Figure S4, SI. Size determination of the trapped beads is easily achieved down to 500 nm from the calibrated optical images [Figure S4(b – e)]. Below this limit, images are influenced by diffraction and become not representative of the actual particle size, but only of the laser spot size. Images like Figure S4(a) are obtained for both 50nm and 90nm samples. Stable 3D trapping of PS spheres is achieved at both wavelengths on particles with $d \geq 500$ nm, provided that the objective pupil is duly overfilled. Conversely, the floating structures visible in the 50 and 90 nm dispersions are always pushed away from the beam focus along the propagation axis, indicating a prevalence of the scattering force over the gradient

one. Stable trapping (2D trapping) is, however, recovered by pushing the particle against the microcell surface, in order to counterbalance the axial pushing force (see schematic in Figure S5, SI). Exploiting this stratagem, we are able to immobilize an analyse very small structures also in the 50 nm and 90 nm samples. Raman spectra of particles optically trapped at 633 nm are shown in Figure 4a (coloured lines indicate different diameters, d = 50 nm – 5 µm) and exhibit the typical fingerprint of PS. Figure S6, SI, displays a zoom of the spectrum acquired on the 50 nm particles, highlighting a good signal to noise ratio ($S/N \sim 3$). Power on the sample is 11 mW and integration times are of the order of tens of seconds. Faster analysis (seconds) can be carried out down to the nanoplastics regime, as shown in the inset of Figure 4a (d = 500 nm, integration time 1 s, $S/N \sim 2$ for the 1000 cm^{-1} band). Better performances are expected, indeed, from more powerful lasers. Optical images of the trapped particles confirm that analysis is, indeed, performed at the single particle level for $d \geq 500$ nm. For the 50 and 90 nm samples, diffraction prevents us from counting the number of particles actually trapped.

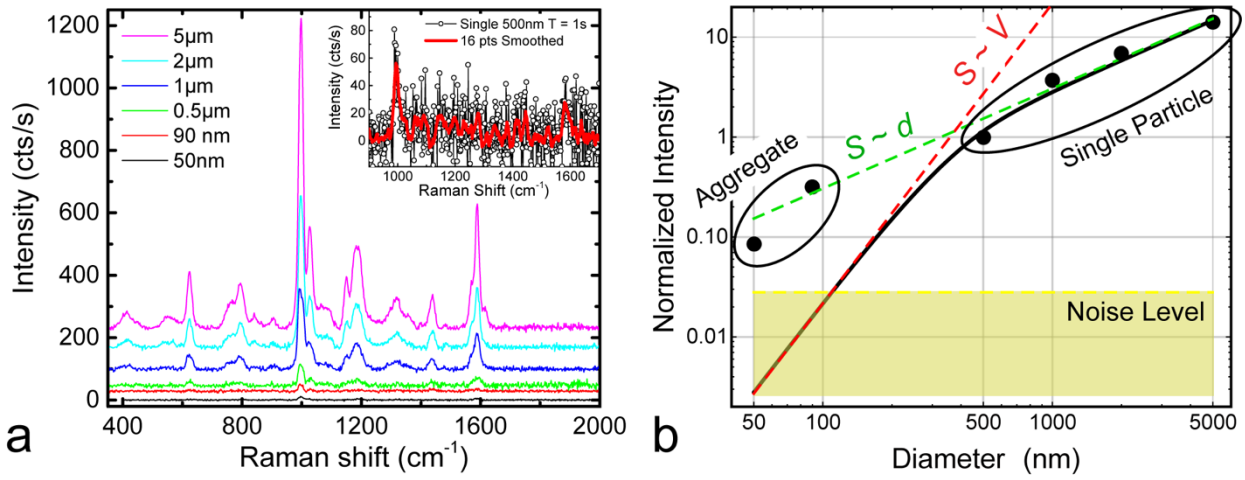

Figure 4: (a) Raman spectra of PS beads (50 nm to 5 µm) optically trapped in distilled water at 633 nm. Power is 11 mW out of the objective. Integration time is T = 10 s (2 acquisitions) for d =

0.5, 1, 2, 5 μm, T = 4 s (2 acquisitions) for d = 90 nm, T = 30 s (2 acquisitions) for d = 50 nm. Spectra plotted in (a) are normalized to the integration time and offset for clarity, after subtraction of the background continuum. This latter signal is typically acquired using integration times 10 times larger in order to reduce its noise contribution to the subtracted spectrum. The inset displays the spectrum (black) and the smoothed curve (red, Savitzky–Golay filter, 16 points) of a 500 nm bead acquired with an integration time of T = 1 s. (b) Normalized Raman signal Vs particles diameter. Experimental data (symbols) are compared to theoretical calculations (black line) for a single trapped particle, and to the trends expected for a particle much smaller than the laser spot, $S \propto V$, (red dashed line) and for a particle much larger than the laser spot, $S \propto d$, (green dashed line). The shadowed area indicates the noise level detected in our measurements for an integration time of 60 s.

Figure 4b(symbols) shows that the Raman signal at 633 nm, S, increases when trapping larger and larger particles. The $S \propto V$ signal dependence [Figure 4b(red dashed line)] is, however, not verified. For particles larger than the laser spot diameter (d_{las} ~ 440 nm) this is expected, since only a limited region of the particle's volume is effectively illuminated (Figure S7), suggesting a sub-volumetric dependence of the Raman signal. A more precise calculation for a single sphere is carried out by integrating the Gaussian intensity profile of a tightly focussed beam over the volume of the sphere, for different diameters (Note S5, SI). The calculated curve [(Figure 4b (black line)] matches well the experimental data for $d \geq$ 500 nm. For large particles ($d \geq$ 1 μm), $S \propto d$ (green dashed line), due to the fact that only the effective volume of the particle intercepted by the light, scaling with d, will give rise to a Raman signal (Figure S7). For the smallest particles ($d \leq$ 300 nm) our model correctly predicts the $S \propto V$ trend (red dashed line). The fact that the experimental signal

330 on the d = 50 and 90 nm trapped structures is more than one order of magnitude larger than that
331 expected for a single particle, suggests that we are trapping aggregates composed of ~ 20 – 30
332 nanoplastics particles. These measurements, however, show the capability of RT to investigate
333 aggregates of the small nanoplastics.

334 Measurements at 785 nm on beads from 90 nm – 2 μm (Figure S8, SI) have been carried out with
335 21 mW power and integration times from 10 to 180 s. The signal (after normalization to power
336 and integration time) turns out to be ca. 4 – 5 times less intense than at 633 nm, due to a worse
337 sensitivity of the detection system in the NIR and to the λ^{-4} wavelength dependence of the Raman
338 scattering. Further advantages at 633 nm are: a smaller power (11 mW against 21 mW at 785 nm),
339 a better signal to noise ratio at equal integration time (50 Vs 30) and a larger spectral range (200-
340 4000 cm^{-1} at 633 nm against 500 – 2500 cm^{-1}) due to the limited response of the detector in the
341 NIR. However, operation at 633 nm induces a signal background due to emission from the soda-
342 lime coverslip, more intense than at 785 nm.

343 Microplastics of different materials (PET, PA6, PVC, PPMA, PP) have been dispersed in distilled
344 water and analysed by RT at 633 nm. The ground particles (PET, PA6, PVC, PPMA) show a size
345 distribution from several tens of microns to the sub-micron scale, with different shapes. The PP
346 particles are quasi-spherical. Most of them have dimensions compatible with the nominal values
347 (11 μm). Smaller particles, from 5 μm down to the sub-micron level are also found. For each
348 material we show in Figure S9, SI, the optical images (a – e) and the Raman spectra (f) of repre-
349 sentative trapped particles, chosen among the smallest found in each sample. The dimensions span
350 from 2 μm (PVC) to ~ 1 μm (PET, PA6), down to the sub-micron scale (PMMA, PP). In all cases
351 we easily identify the nature of the trapped particles using the reference spectra.

Detection and identification of micro- and nanoplastics in seawater. RT operation in seawater is somehow complicated by (i) the presence of a more intense background; (ii) the tendency of the smallest particles to form homo- and/or hetero-aggregates; (iii) the presence of microorganisms and mineral particles in the sediments dispersed in seawater. Background at 633 nm (Figure S10a, black line, SI) is 10 times more intense than in distilled water, probably due to substances dissolved therein. At 785 nm the background (Figure S10a, green line, SI) consists of two small peaks before 1000 cm^{-1} and a broad band at ~ 1450 cm^{-1} that originates from the fluorescence of the soda-lime coverslip. At both wavelengths, however, chemical identification of optically trapped PE particles of few microns diameter is straightforward and unambiguous (Figure S10a, red and blue lines), especially after background subtraction (Figure S7b, red and blue lines). Raman spectra of optically trapped particles in seawater of common plastic pollutants are shown in Figure 5, together with their optical images. The particles feature dimensions in the micrometre (PET, PVC, PP, PE) and sub-micron scale (PMMA, PA6) and have been chosen among the smallest found in each solution. Measurements at 633 nm require integration times from 2 s to 60 s. Unambiguous Raman signatures are found for all the micro and nanoplastics analysed.

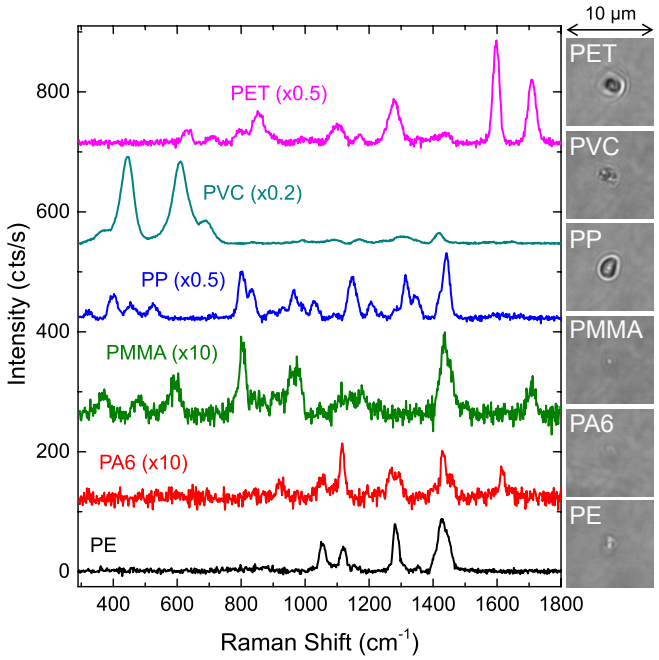

Figure 5: Raman spectra of optically trapped micro- and nano- plastics made of different materials, dispersed in seawater. Particles dimensions are: PET 2.6 µm, PVC 3 µm, PP 2.8 µm, PMMA sub-micron, PA6: sub-micron, PE 2 µm. Laser wavelength 633 nm. Power 11 mW out of the objective. Integration times are 20 s (2 acquisitions) for PE and PVC, 60 s (2 acquisitions) for PA6 and PMMA, 4 s (2 acquisitions) for PP, and 2 s (2 acquisitions) for PET. Spectra are background-subtracted, rescaled (factors indicated in parentheses) and offset for clarity.

Detection of single nanoplastics in seawater. The use of commercial nanobeads as model systems for environmental studies has been questioned[22] due to their artificial origin and the different physical/chemical properties with respect to nanoplastics originating from the natural degradation of microplastics (e.g. random shapes, polydisperse dimensions, …). In particular, it is pointed out that nanoplastics form homo- or hetero-aggregates with other natural or man-produced particles. We have carried out experiments on 300 nm PMMA beads and 90 nm PS beads in seawater.

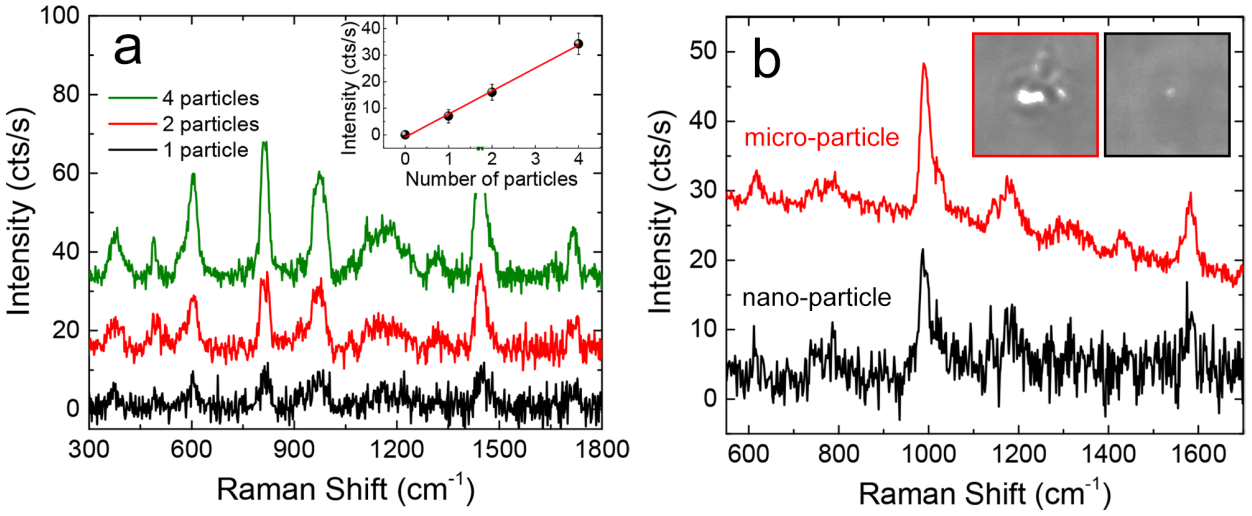

Figure 6: (a) Background subtracted spectra of 1, 2 and 4 PMMA particles (d = 300 nm) optically trapped at 633 nm (power 11 mW, integration 10 s, 6 acquisitions). Inset: intensity of the 810 cm^{-1} mode Vs number of particles (symbols) and linear fit (red line) of the data. (b) Raman spectra of a micrometric (red line) and of a nanometric (black line) PS particle (d = 90 nm) optically trapped at 633 nm (power 11 mW, integration time 60 s, 2 acquisitions). Spectra are normalized to the integration time, so that the intensities are directly comparable. Insets: optical images of the particles (images size 5×5 μm^2).

Figure 6a shows the Raman signal of n_p = 1, 2, and 4 PMMA particles stably trapped in 3D at 633 nm. The particles can be individually counted after being released from the trap (Movie S3, SI). For n_p = 4, we see two individual particles and a dimer. The intensity of 810 cm^{-1} Raman band (inset of Figure 6a) increases linearly with n_p, confirming that the dimer is a PMMA homodimer. Individual PMMA nanoparticles are clearly identified with a S/N ratio ~ 4 in 60 s integration time. The PS particles, stable for months in distilled water, aggregate into micron scale structures after few minutes from dispersion in seawater.[80] Upon addition of a drop of surfactant and vigorous shaking, however, nanoscale PS structures can be observed in the dispersions. Figure 6b (insets) shows the optical pictures (5×5 μm^2) and the Raman spectra of a micron scale (red line) and a

399 nanoscale (black line) particle optically trapped in 2D at 633 nm, present, respectively, in the nat-
400 ural dispersion and in that with the surfactant. The signal intensity of the nanoparticle (black) is
401 similar to what expected from an aggregate of ~ 35 particles. The micron scale particle is charac-
402 terized by a continuum background (not related to glass) on which the Raman peaks are superim-
403 posed. The intensity on the 1000 cm^{-1} peak is only 1.5 time more intense than on the nanoparticle,
404 in spite of a much larger volume. This suggests that we are probably trapping a hetero-aggregate
405 composed of about 50 PS particles bound to some slightly fluorescent larger structure.

406

407 Artificially aged PE particles covered with organic over-layers. RT have been used to detect PE
408 microparticles that have undergone ageing in seawater. Two samples are studied, one of them
409 covered with a biosurfactant from microalgae exudates.[79] Raman spectra of optically trapped par-
410 ticles between 0.7 μm and 2 μm display the characteristic bands of PE (Figure 7). The higher
411 intensities generally measured in the seawater sample, are maybe due to the presence of homo-
412 aggregates or particles larger than those present in the sample with the biosurfactant. No Raman
413 fingerprint of this latter molecule is detected, indicating that plastics can be identified despite the
414 presence of an eco-corona, too thin to be detected. Finally, we have optically trapped particles in
415 both samples that do not provide any Raman signal (Figure 7, cyan and black lines), although we
416 set an acquisition time as long as 300 s. These maybe microorganisms present in the seawater.

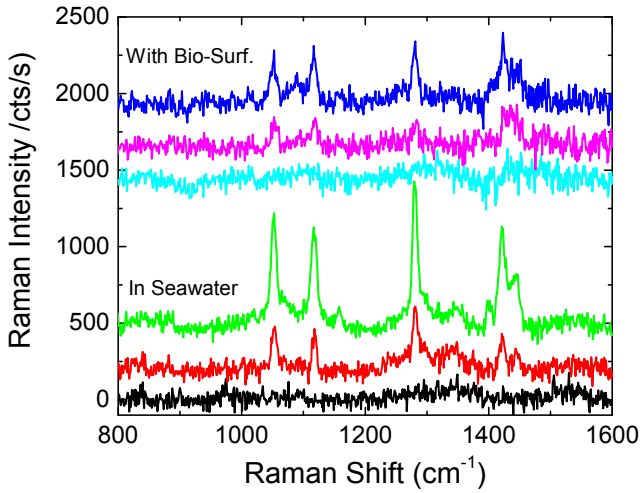

Figure 7. Background-subtracted Raman spectra of PE particles optically trapped in seawater without (red, green) and in presence of the biosurfactant (blue, magenta). Laser wavelength 785 nm, power 21 mW, integration time 300 s, 3 acquisitions. In both samples we found particles that, upon trapping, do not provide any Raman signal (cyan and black lines) even after 15 min integration time.

Marine sediments. Marine sediments in form of micro and nanoparticles have been optically trapped and analysed in seawater samples (Figure 8), in order to acquire a reference database of the species present in the hosting liquid and allow for unambiguous monitoring of plastic particles in presence of sediments.[81] Modes assignment is reported in Note S6, SI. Several minerals are found, such as Anatase (pink), Laumontite (blue), Calcite (which was the most common, green). and Alginate (red). In addition, we find particles of Alginate (red) and spectra that we attribute to hetero aggregates of Hematite-Jarosite (dark green) and Hematite-Alginate (black).

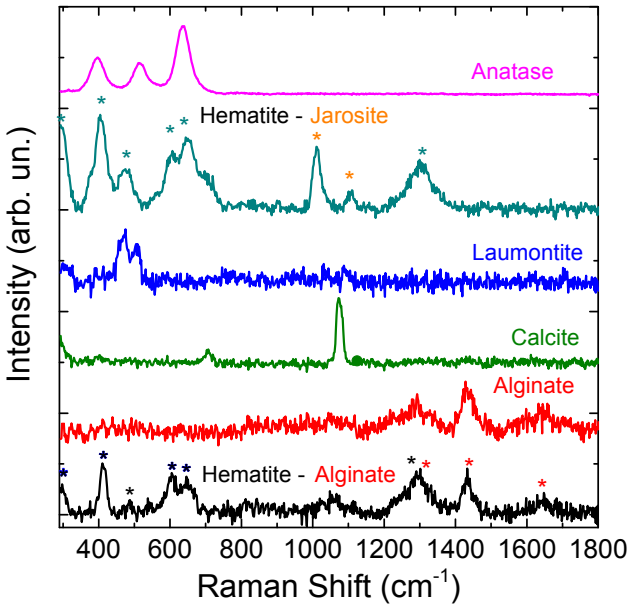

Figure 8. Raman spectra of different sediments dispersed in sea water optically trapped. Asterisks dark green asterisks in the Hematite-Jarosite spectrum (dark green line) indicate the Hematite modes. The orange ones refer to Jarosite. The black asterisks in the Hematite-Alginate spectrum (black line) indicate the hematite modes, the red asterisks the Alginate modes. Excitation wavelength 633 nm, power 11 mW, integration time 20 s, 2 acquisitions. Particles dimensions are: anatase 8 µm, hematite-Jarosite 20 µm, Laumontite 7 µm, calcite < 1 µm, alginate 1 µm, hematite-alginate 1.4 µm.

Detection of Nylon fibres in PP samples. Experiments on commercial PP particles dispersed in seawater allow us to show unambiguous chemical discrimination of different microplastics. Figure 9(a) displays a micrometric fibre found in a sample of spheroidal PP particles (b). The Raman signatures (c, blue and red lines) compared to the reference spectra (green and black lines) allow us to conclude that the spheroidal particle is made of PP, as expected, whereas the fibre is composed mostly of nylon. Some weaker peaks (indicated with red asterisks) are compatible with the

presence of smaller PP particles, suggesting the occurrence of a hetero-aggregate. The origin of the nylon fiber in the sample is unknown. Some textile fibres could have been accidentally mixed to the PP during fabrication, or maybe the fibre was already present in the seawater sample. This is a very interesting result, since micro and nanofibers are suspected to be prevalent in the aquatic environment whereas their detection and identification remains particularly challenging.[8,34]

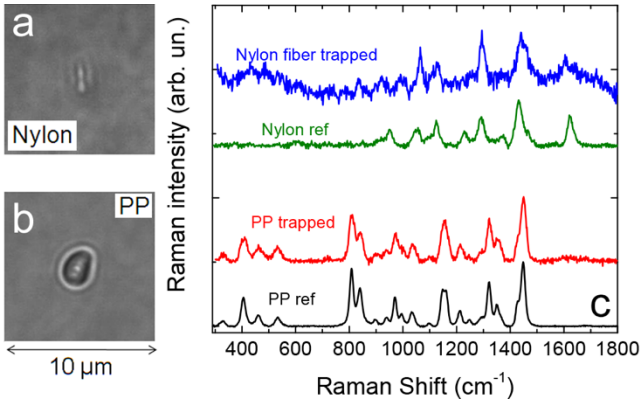

Figure 9. Optical images of (a) a nylon fiber and (b) a spheroidal PP particle dispersed in seawater. (c) Raman spectra of the optically trapped particles (blue and red) compared with the reference spectra (green and black lines) acquired on bulk samples. The red asterisks highlight additional peaks in the nylon spectrum that can be attributed to PP. Excitation wavelength 633 nm, power 11 mW, integration times 4 s, 2 acquisitions.

Naturally aged PE and PP plastics. Mechanical shock and stress applied to aged plastics, brittle because of weathering-induced crystallization, causes the release of microplastics in the environment. Typical situations are those in which plastic litter impacts against the rocks or it is stepped on, or shattered during cleaning operations or collection in open sea. Indeed, the degree and scale of fragmentation depend on ageing time, weathering conditions and polymer nature. We have first analysed the fragmentation of a naturally aged PE bottle cap. Upon application of a mechanical

pressure, it spontaneously breaks into millimetric and sub-millimetric debris (Figure 10a). Part of the cap has then been broken in seawater, and the resulting solution analysed by trapping the floating particles with RT (spectra are displayed in Figure 10b, optical images in c – e). As expected, we find several PE fragments some of which have dimensions as small as few microns (Figure 10b, black line and Figure 10e).

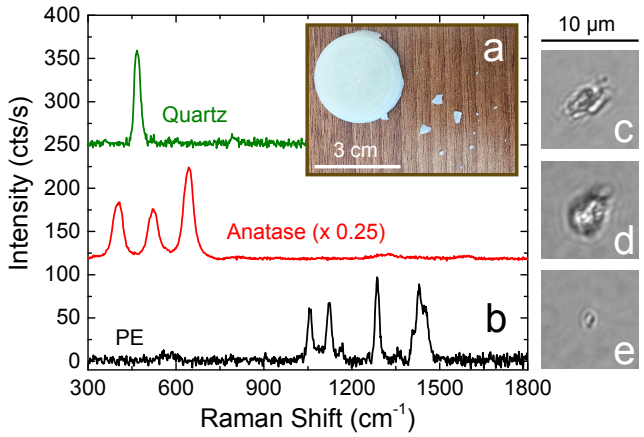

Figure 10. (a) Picture of a naturally aged PE bottle cap and of the fragments generated after its breaking. (b) Raman spectra of optically trapped particles obtained from fragmentation of the cap in seawater, alongside with their images: (c) quartz particle (7.2 µm), (d) anatase particle (6.5 µm), (e) PE microplastic (2.3 µm). Laser wavelength 633 nm, acquisition time 10s (2 acquisitions).

Together with plastics, microscopic anatase particles are detected (Figure 10b, red line and Figure 10d), probably due to residual sediments, as well as microscopic quartz particles (Figure 10b, green line and Figure 10c), probably sand, that can be identified by its Raman signature[82] dominated by a peak at 467 cm^{-1}, followed by a small band at 800 cm^{-1} and preceded by a small band at 358 cm^{-1}.

We have finally investigated the microplastics release arising from the crushing of an old, naturally aged PP bucket (Figure 11a). Figure 11b shows the fragmentation level of a cm scale piece broken in air highlighting the presence of debris with dimensions from the mm to the sub-mm (micrometric) scale. Microscopy images (Figure 11c) show that the fragmentation level reaches the micrometric and even the sub-micrometric scale. MicroRaman spectra (not shown) confirmed the PP nature of the fragments. A piece of bucket was then broken in seawater and the chemical nature and size of the debris analysed by RT (d) and optical microscopy (e – j). Apart from the expected large presence of PP microparticles, we have detected few PP particles with nanoscale size, as the one shown in Figure 11j which is ~ 750 nm large, and whose spectrum is displayed in Figure 11d (black line). Together with this, we find micrometric rutile particles, both pure and in form of hetero-aggregates with PP (red and green lines), originating from the residual paint in the inner wall (Fig. S12, SI). Amorphous carbon particles, also in combination with PP (magenta and orange lines), are observed. They have been trapped in 2D because of the high radiation pressure due to strong light absorption. The origin of such particles is probably related to traces of carbon-based contaminants. Finally, we find particles that display the spectral fingerprint of β-carotene, characterized by intense bands at 1510 cm^{-1} (νC=C) 1148 cm^{-1} (νC-C) and 1000 cm^{-1} (νC-CH_3). These are likely algae[83] absorbed at the surface of the bucket.

The analysis reported so far is, indeed, enabled by the capabilities of RT to work at the single particle level. Spectra on liquid dispersions of PP with configurations typical of Raman spectroscopy in liquid (e.g. using a 10X objective) did not provide any detectable plastics signal (Note S6, Figure S11, SI).

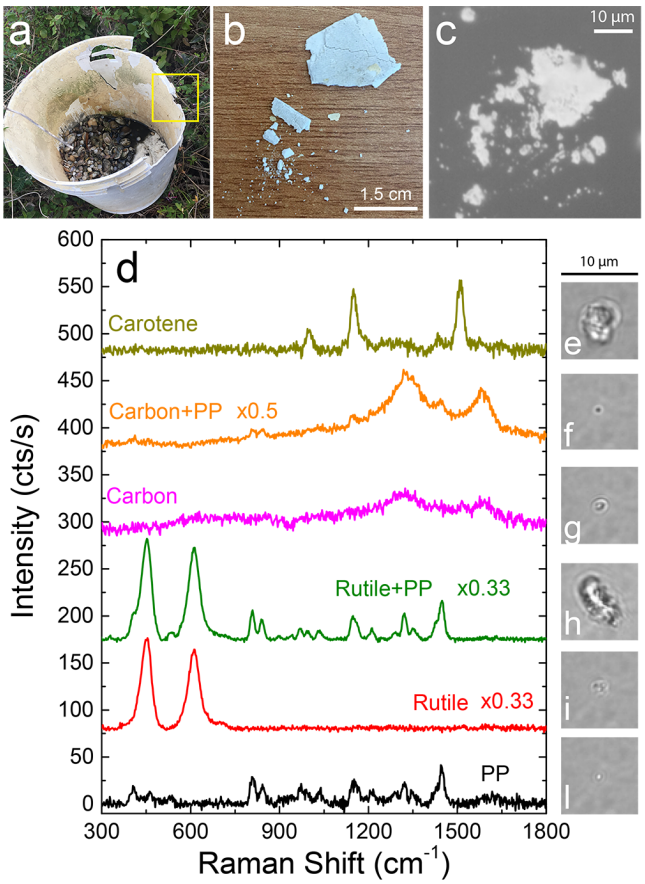

Figure 11: (a) Picture of a PP paint bucket naturally aged, from which we have extracted our samples (the yellow box indicates the zone which has been sampled). (b) Typical fragments generated when a piece of bucket is broken. (c) Microscope image of a fragment of PP and its smaller debris. (d) Raman spectra of optically trapped particles obtained from fragmentation of pieces of the bucket in seawater, alongside with their images: (e) carotene particle (6.4µm), (f) amorphous carbon mixed with PP (1.2 µm), (g) amorphous carbon particle (1.8 µm), (h) rutile and PP heteroaggregate (6.7 µm), (i) rutile particle (2.2 µm), (j) PP nanoplastic particle (0.75 µm). Laser wavelength 633 nm, power 11 mW, acquisition time 10 s, 2 acquisitions.

In conclusion, we have applied RTs for chemical qualitative analysis of different plastic particles with sizes in the sub-20 μm fraction in seawater. Aggregates of some tens of nanoparticles with diameter of 50 nm and 90 nm (small nanoplastics) can be trapped and detected, as well as individual PMMA nanoplastics of 300 nm diameter and larger particles of PS and other common pollutants. RTs enable analysis at the single particle level, overcoming the limitations of conventional Raman spectroscopy in liquid. Optical images provide information on the size of the trapped particles down to ~ 500 nm, whereas the Raman spectra permit unambiguous chemical identification of the different materials, even in presence of thin organic over-layers. Discrimination of PP microplastics from small microfibers in seawater is shown. Fast analysis (few seconds to few tens of seconds per spectrum) is achieved exciting in at 633 nm with powers of 11 mW. NIR lasers (785 nm) require longer analysis times (10 to 100 times). Raman fingerprints from micrometric and sub-micrometric marine sediments have been acquired, and they could be unambiguously distinguished from plastics. Experiments on PP and PE particles extracted from naturally aged plastic litter show that RTs can be used to identify nanoplastics that would be present in a marine sample. Furthermore, RTs appear as a suitable tool to study the degree of release of micro and nanoplastics in the aquatic environment through fragmentation of macro and microplastics, mechanisms that are still not well understood. Thanks to the chemical discrimination capabilities, we could here unambiguously show that accidental fragmentation of old PP and PE objects is a source of small microplastics and, for the case of PP, also of nanoplastics.

RTs, as all other analytical techniques capable to operate at the single particle level (μRaman, μFTIR, …), require concentrated samples. Experiments on model particles show that concentrations of ~ 10^4 – 10^5 particles per mL are required in order to easily spot, trap and analyse the samples. Such a high density can be potentially reduced by a factor 100 using wide field objectives

(5X or 10X) to spot the particles and then switch to a 100X objective for trapping and analysis. A strong experimental effort in terms of particles concentration is, however, needed for applications in marine research. RTs is a spectroscopic tool capable to study the fate of micro and nanoplastics in marine environments and to determine the effect of ageing and fragmentation on plastic materials. Future experimental developments should be directed towards quantitative analysis, through the implementation of RT for liquid flow operation in suitable microfluidic cells,[84,85,86] artificial intelligence routines to spot, count and analyse the nature particles, and adopt big data analysis tools to treat the thousands of spectra required to provide reliable particles size distributions of different polymeric materials.

Supporting Information.

Movie S1 and S2 show the optical trapping, manipulation and optically-induced rotation of spherical and non-spherical microplastics. Movie S3 shows the trapping and release of 1, 2, 4 PMMA particles in seawater. Additional notes and tables on: micro and nanoplastics definitions, optical forces calculations, thermodynamic-related issues on nanoplastics trapping, refractive index of common plastic pollutants, Raman modes assignment for most common plastic pollutants, calculation of the Raman signal in an optical trap, Raman modes assignment of mineral sediments, Raman spectroscopy in liquid. Additional figures on: optical forces calculations on 10 μm PE beads and 90 nm PS beads, trapping power threshold for nanoplastics, Raman spectra of common plastics, schematic of 2D trapping, spectrum of 50 nm particles aggregate optically trapped, schematic of the model used to calculate the Raman scattering in a RT, Raman spectra of optically trapped PS beads at 785 nm, background signal on the Raman signal of microplastics at 633 and 785 nm in distilled water and seawater, Raman spectra of several optically trapped micro and

nanoplastics in distilled water, conventional Raman spectroscopy of sparse PP microplastics in seawater.

AUTHOR INFORMATION

Corresponding Author

Pietro G. Gucciardi. Address: CNR – IPCF, Istituto per i Processi Chimico-Fisici, Viale F. Stagno D'Alcontres 27, I- 98158 Messina, Italy. Tel. +39 090 39762 248. Email: guc-ciardi@ipcf.cnr.it

ORCID

Raymond Gillibert: 0000-0003-4318-6346

Florent Colas: 0000-0002-9882-3720

Gireeshkumar Balakrishnan: 0000-0002-1648-8149

Quentin Deshoules: 0000-0002-2014-5026

Morgan Tardivel: 0000-0002-9591-2138

Alessandro Magazzù: 0000-0003-1247-2702

Maria Grazia Donato: 0000-0002-7580-3137

Onofrio M. Maragò: 0000-0002-7220-8527

Marc Lamy de La Chapelle:

Fabienne Lagarde: 0000-0002-4015-4376

Pietro G. Gucciardi: 0000-0003-1826-9174

NOTES

The authors declare no competing financial interests.

ACKNOWLEDGMENTS

This work has been funded by IFREMER through the project MERLIN-MICROPLASTIQUE (convention 17/1212947B). Partial economical funding from the Joint Bilateral Agreement CNR/The Czech Academy of Sciences (CAS), Triennial Programme 2016-2018 is also acknowledged. E. Rinnert and A. Huvet are acknowledged for the careful reading of the paper and fruitful comments. V. Villari and N. Micali are acknowledged for providing the 90 nm PS particles. G Di Marco is acknowledged for fruitful discussions. Two H Chem ltd is acknowledged for providing the PP samples.

TOC/ABSTRACT ART

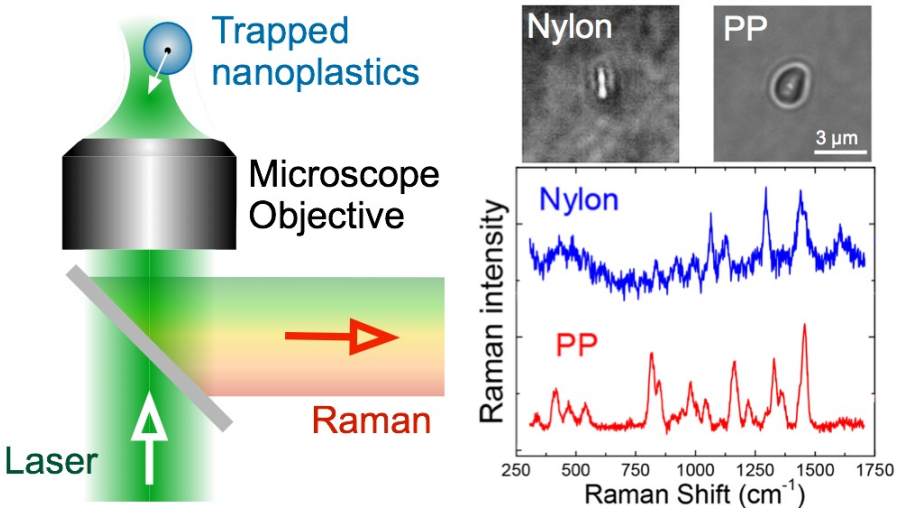

593 REFERENCES

594

[1] Carpenter, E. J.; Anderson, S. J.; Harvey, G. R.; Miklas, H. P.; Peck, B. B. Polystyrene Spherules in Coastal Waters. *Science* **1972**, *178* (4062), 749–750. https://doi.org/10.1126/science.178.4062.749

[2] Hurley, R.; Woodward, J.; Rothwell, J. J. Microplastic Contamination of River Beds Significantly Reduced by Catchment-Wide Flooding. *Nat. Geosci.* **2018**, *11* (4), 251–257. https://doi.org/10.1038/s41561-018-0080-1

[3] ter Halle, A.; Jeanneau, L.; Martignac, M.; Jardé, E.; Pedrono, B.; Brach, L.; Gigault, J. Nanoplastic in the North Atlantic Subtropical Gyre. *Environ. Sci. Technol.* **2017**, *51* (23), 13689–13697. https://doi.org/10.1021/acs.est.7b03667

[4] Thompson, R. C.; Olsen, Y.; Mitchell, R. P.; Davis, A.; Rowland, S. J.; John, A. W. G.; McGonigle, D.; Russell, A. E. Lost at Sea: Where Is All the Plastic? *Science* **2004**, *304* (5672), 838–838. https://doi.org/10.1126/science.1094559

[5] Andrady, A. L. Microplastics in the Marine Environment. *Mar. Pollut. Bull.* **2011**, *62* (8), 1596–1605. https://doi.org/10.1016/j.marpolbul.2011.05.030

[6] da Costa, J. P.; Santos, P. S. M.; Duarte, A. C.; Rocha-Santos, T. (Nano)Plastics in the Environment – Sources, Fates and Effects. *Sci. Total Environ.* **2016**, *566–567*, 15–26. https://doi.org/10.1016/j.scitotenv.2016.05.041

[7] Ng, E.-L.; Huerta Lwanga, E.; Eldridge, S. M.; Johnston, P.; Hu, H.-W.; Geissen, V.; Chen, D. An Overview of Microplastic and Nanoplastic Pollution in Agroecosystems. *Sci. Total Environ.* **2018**, *627*, 1377–1388. https://doi.org/10.1016/j.scitotenv.2018.01.341

[8] Salvador Cesa, F.; Turra, A.; Baruque-Ramos, J. Synthetic Fibers as Microplastics in the Marine Environment: A Review from Textile Perspective with a Focus on Domestic Washings. *Sci. Total Environ.* **2017**, *598*, 1116–1129. https://doi.org/10.1016/j.scitotenv.2017.04.172.

[9] Koelmans, A. A.; Besseling, E.; Shim, W. J. Nanoplastics in the Aquatic Environment. Critical Review. In *Marine Anthropogenic Litter*; Bergmann, M., Gutow, L., Klages, M., Eds.; Springer International Publishing: Cham, 2015; pp 325–340. https://doi.org/10.1007/978-3-319-16510-3_12.

[10] Farrell, P.; Nelson, K. Trophic Level Transfer of Microplastic: Mytilus Edulis (L.) to Carcinus Maenas (L.). *Environ. Pollut.* **2013**, *177*, 1–3. https://doi.org/10.1016/j.envpol.2013.01.046.

[11] Setälä, O.; Fleming-Lehtinen, V.; Lehtiniemi, M. Ingestion and Transfer of Microplastics in the Planktonic Food Web. *Environ. Pollut.* **2014**, *185*, 77–83. https://doi.org/10.1016/j.envpol.2013.10.013

[12] Phuong, N. N.; Zalouk-Vergnoux, A.; Kamari, A.; Mouneyrac, C.; Amiard, F.; Poirier, L.; Lagarde, F. Quantification and Characterization of Microplastics in Blue Mussels (Mytilus Edulis): Protocol Setup and Preliminary Data on the Contamination of the French Atlantic Coast. *Environ. Sci. Pollut. Res.* **2018**, *25* (7), 6135–6144. https://doi.org/10.1007/s11356-017-8862-3.

[13] Wright, S. L.; Kelly, F. J. Plastic and Human Health: A Micro Issue? *Environ. Sci. Technol.* **2017**, *51* (12), 6634–6647. https://doi.org/10.1021/acs.est.7b00423.

[14] Revel, M.; Châtel, A.; Mouneyrac, C. Micro(Nano)Plastics: A Threat to Human Health? *Curr. Opin. Environ. Sci. Health* **2018**, *1*, 17–23. https://doi.org/10.1016/j.coesh.2017.10.003.

[15] Cózar, A.; Echevarría, F.; González-Gordillo, J. I.; Irigoien, X.; Úbeda, B.; Hernández-León, S.; Palma, Á. T.; Navarro, S.; García-de-Lomas, J.; Ruiz, A. Plastic Debris in the Open Ocean. *Proc. Natl. Acad. Sci.* **2014**, *111* (28), 10239–10244

[16] Erni-Cassola, G.; Gibson, M. I.; Thompson, R. C.; Christie-Oleza, J. A. Lost, but Found with Nile Red: A Novel Method for Detecting and Quantifying Small Microplastics (1 mm to 20 μm) in Environmental Samples. *Environ. Sci. Technol.* **2017**, *51* (23), 13641–13648. https://doi.org/10.1021/acs.est.7b04512

[17] Suaria, G.; Avio, C. G.; Mineo, A.; Lattin, G. L.; Magaldi, M. G.; Belmonte, G.; Moore, C. J.; Regoli, F.; Aliani, S. The Mediterranean Plastic Soup: Synthetic Polymers in Mediterranean Surface Waters. *Sci. Rep.* **2016**, *6*, 37551

[18] Eo, S.; Hong, S. H.; Song, Y. K.; Lee, J.; Lee, J.; Shim, W. J. Abundance, Composition, and Distribution of Microplastics Larger than 20 μm in Sand Beaches of South Korea. *Environ. Pollut.* **2018**, *238*, 894–902. https://doi.org/10.1016/j.envpol.2018.03.096

[19] Pivokonsky, M.; Cermakova, L.; Novotna, K.; Peer, P.; Cajthaml, T.; Janda, V. Occurrence of Microplastics in Raw and Treated Drinking Water. *Sci. Total Environ.* **2018**, *643*, 1644–1651. https://doi.org/10.1016/j.scitotenv.2018.08.102

[20] Cincinelli, A.; Scopetani, C.; Chelazzi, D.; Lombardini, E.; Martellini, T.; Katsoyiannis, A.; Fossi, M. C.; Corsolini, S. Microplastic in the Surface Waters of the Ross Sea (Antarctica):

Occurrence, Distribution and Characterization by FTIR. *Chemosphere* **2017**, *175*, 391–400. https://doi.org/10.1016/j.chemosphere.2017.02.024.

[21] Cole, M.; Lindeque, P.; Fileman, E.; Halsband, C.; Goodhead, R.; Moger, J.; Galloway, T. S. Microplastic Ingestion by Zooplankton. *Environ. Sci. Technol.* **2013**, 47 (12), 6646–6655. https://doi.org/10.1021/es400663f.

[22] Gigault, J.; ter Halle, A.; Baudrimont, M.; Pascal, P.-Y.; Gauffre, F.; Phi, T.-L.; El Hadri, H.; Grassl, B.; Reynaud, S. Current Opinion: What Is a Nanoplastic? *Environ. Pollut.* **2018**, *235*, 1030–1034. https://doi.org/10.1016/j.envpol.2018.01.024

[23] Gigault, J.; Pedrono, B.; Maxit, B.; Halle, A. T. Marine Plastic Litter: The Unanalyzed Nano-Fraction. *Environ. Sci. Nano* **2016**, *3* (2), 346–350. https://doi.org/10.1039/C6EN00008H

[24] Lambert, S.; Wagner, M. Characterisation of Nanoplastics during the Degradation of Polystyrene. *Chemosphere* **2016**, *145*, 265–268. https://doi.org/10.1016/j.chemosphere.2015.11.078

[25] Dawson, A. L.; Kawaguchi, S.; King, C. K.; Townsend, K. A.; King, R.; Huston, W. M.; Nash, S. M. B. Turning Microplastics into Nanoplastics through Digestive Fragmentation by Antarctic Krill. *Nat. Commun.* **2018**, *9* (1), 1001. https://doi.org/10.1038/s41467-018-03465-9.

[26] Cole, M.; Galloway, T. S. Ingestion of Nanoplastics and Microplastics by Pacific Oyster Larvae. *Environ. Sci. Technol.* **2015**, *49* (24), 14625–14632. https://doi.org/10.1021/acs.est.5b04099

[27] Tallec, K.; Huvet, A.; Di Poi, C.; González-Fernández, C.; Lambert, C.; Petton, B.; Le Goïc, N.; Berchel, M.; Soudant, P.; Paul-Pont, I. Nanoplastics Impaired Oyster Free Living Stages, Gametes and Embryos. *Environ. Pollut.* **2018**, *242*, 1226–1235. https://doi.org/10.1016/j.envpol.2018.08.020.

[28] Hidalgo-Ruz, V.; Gutow, L.; Thompson, R. C.; Thiel, M. Microplastics in the Marine Environment: A Review of the Methods Used for Identification and Quantification. *Environ. Sci. Technol.* **2012**, *46* (6), 3060–3075. https://doi.org/10.1021/es2031505.

[29] Rocha-Santos, T.; Duarte, A. C. A Critical Overview of the Analytical Approaches to the Occurrence, the Fate and the Behavior of Microplastics in the Environment. *TrAC Trends Anal. Chem.* **2015**, *65*, 47–53. https://doi.org/10.1016/j.trac.2014.10.011.

[30] Galgani, F.; Hanke, G.; Werner, S.; Oosterbaan, L.; Nilsson, P.; Fleet, D.; Kinsey, S.; Thompson, R.; van Franeker, J.; Vlachogianni, T.; Scoullos, M.; Veiga, J.; Palatinus, A.; Matiddi, M.; Maes, T.; Korpinen, S.; Budziak, A.; Leslie, H.; Gago, J.; Liebezeit, G. Guidance on monitoring of marine litter in European seas. report. Institute for Environment and Sustainability; **2013**.

[31] Renner, G.; Schmidt, T. C.; Schram, J. Analytical Methodologies for Monitoring Micro(Nano)Plastics: Which Are Fit for Purpose? *Curr. Opin. Environ. Sci. Health* **2018**, *1*, 55–61. https://doi.org/10.1016/j.coesh.2017.11.001.

[32] Primpke, S.; Lorenz, C.; Rascher-Friesenhausen, R.; Gerdts, G. An Automated Approach for Microplastics Analysis Using Focal Plane Array (FPA) FTIR Microscopy and Image Analysis. *Anal. Methods* **2017**, *9* (9), 1499–1511. https://doi.org/10.1039/C6AY02476A

[33] Käppler, A.; Fischer, D.; Oberbeckmann, S.; Schernewski, G.; Labrenz, M.; Eichhorn, K.-J.; Voit, B. Analysis of Environmental Microplastics by Vibrational Microspectroscopy: FTIR, Raman or Both? *Anal. Bioanal. Chem.* **2016**, *408* (29), 8377–8391. https://doi.org/10.1007/s00216-016-9956-3

[34] Mintenig, S. M.; Int-Veen, I.; Löder, M. G. J.; Primpke, S.; Gerdts, G. Identification of Microplastic in Effluents of Waste Water Treatment Plants Using Focal Plane Array-Based Micro-Fourier-Transform Infrared Imaging. *Water Res.* **2017**, *108*, 365–372. https://doi.org/10.1016/j.watres.2016.11.015.

[35] Frère, L.; Paul-Pont, I.; Moreau, J.; Soudant, P.; Lambert, C.; Huvet, A.; Rinnert, E. A Semi-Automated Raman Micro-Spectroscopy Method for Morphological and Chemical Characterizations of Microplastic Litter. *Mar. Pollut. Bull.* **2016**, *113* (1), 461–468. https://doi.org/10.1016/j.marpolbul.2016.10.051

[36] Araujo, C. F.; Nolasco, M. M.; Ribeiro, A. M. P.; Ribeiro-Claro, P. J. A. Identification of Microplastics Using Raman Spectroscopy: Latest Developments and Future Prospects. *Water Res.* **2018**, *142*, 426–440. https://doi.org/10.1016/j.watres.2018.05.060.

[37] Dekiff, J. H.; Remy, D.; Klasmeier, J.; Fries, E. Occurrence and Spatial Distribution of Microplastics in Sediments from Norderney. *Environ. Pollut.* **2014**, *186*, 248–256. https://doi.org/10.1016/j.envpol.2013.11.019.

[38] Fries, E.; Dekiff, J. H.; Willmeyer, J.; Nuelle, M.-T.; Ebert, M.; Remy, D. Identification of Polymer Types and Additives in Marine Microplastic Particles Using Pyrolysis-GC/MS and Scanning Electron Microscopy. *Environ. Sci. Process. Impacts* **2013**, *15* (10), 1949–1956. https://doi.org/10.1039/C3EM00214D

[39] Käppler, A.; Fischer, M.; Scholz-Böttcher, B. M.; Oberbeckmann, S.; Labrenz, M.; Fischer, D.; Eichhorn, K.-J.; Voit, B. Comparison of μ-ATR-FTIR Spectroscopy and Py-GCMS as Identification Tools for Microplastic Particles and Fibers Isolated from River Sediments. *Anal. Bioanal. Chem.* **2018**, *410* (21), 5313–5327. https://doi.org/10.1007/s00216-018-1185-5.

[40] Dümichen, E.; Eisentraut, P.; Bannick, C. G.; Barthel, A.-K.; Senz, R.; Braun, U. Fast Identification of Microplastics in Complex Environmental Samples by a Thermal Degradation Method. *Chemosphere* **2017**, *174*, 572–584. https://doi.org/10.1016/j.chemosphere.2017.02.010

[41] Maes, T.; Jessop, R.; Wellner, N.; Haupt, K.; Mayes, A. G. A Rapid-Screening Approach to Detect and Quantify Microplastics Based on Fluorescent Tagging with Nile Red. *Sci. Rep.* **2017**, *7*, 44501. https://doi.org/10.1038/srep44501

[42] da Costa, J. P. Micro- and Nanoplastics in the Environment: Research and Policymaking. *Curr. Opin. Environ. Sci. Health* **2018**, *1*, 12–16. https://doi.org/10.1016/j.coesh.2017.11.002

[43] Peiponen, K.-E.; Räty, J.; Ishaq, U.; Pélisset, S.; Ali, R. Outlook on Optical Identification of Micro- and Nanoplastics in Aquatic Environments. *Chemosphere* **2019**, *214*, 424–429. https://doi.org/10.1016/j.chemosphere.2018.09.111.

[44] Schwaferts, C.; Niessner, R.; Elsner, M.; Ivleva, N. P. Methods for the Analysis of Submicrometer- and Nanoplastic Particles in the Environment. *TrAC Trends Anal. Chem.* **2019**, *112*, 52–65. https://doi.org/10.1016/j.trac.2018.12.014

[45] *Raman Spectroscopy for Nanomaterials Characterization*; Kumar, C. S. S. R., Ed.; Springer-Verlag: Berlin Heidelberg, 2012

[46] Dresselhaus, M. S.; Dresselhaus, G.; Jorio, A.; Souza Filho, A. G.; Saito, R. Raman Spectroscopy on Isolated Single Wall Carbon Nanotubes. *Carbon* **2002**, *40* (12), 2043–2061. https://doi.org/10.1016/S0008-6223(02)00066-0

[47] Ferrari, A. C.; Meyer, J. C.; Scardaci, V.; Casiraghi, C.; Lazzeri, M.; Mauri, F.; Piscanec, S.; Jiang, D.; Novoselov, K. S.; Roth, S.; Geim, A. K. Raman Spectrum of Graphene and Graphene Layers. *Phys. Rev. Lett.* **2006**, *97* (18), 187401. https://doi.org/10.1103/PhysRevLett.97.187401.

[48] Dorney, J.; Bonnier, F.; Garcia, A.; Casey, A.; Chambers, G.; J. Byrne, H. Identifying and Localizing Intracellular Nanoparticles Using Raman Spectroscopy. *Analyst* **2012**, *137* (5), 1111–1119. https://doi.org/10.1039/C2AN15977E.

[49] Dazzi, A.; Prater, C. B. AFM-IR: Technology and Applications in Nanoscale Infrared Spectroscopy and Chemical Imaging. *Chem. Rev.* **2017**, *117* (7), 5146–5173. https://doi.org/10.1021/acs.chemrev.6b00448

[50] Gucciardi, P. G.; Trusso, S.; Vasi, C.; Patanè, S.; Allegrini, M. Near-Field Raman Spectroscopy and Imaging. In *Applied Scanning Probe Methods V: Scanning Probe Microscopy Techniques*; Bhushan, B., Kawata, S., Fuchs, H., Eds.; NanoScience and Technology; Springer Berlin Heidelberg: Berlin, Heidelberg, 2007; pp 287–329. https://doi.org/10.1007/978-3-540-37316-2_10

[51] Huth, F.; Schnell, M.; Wittborn, J.; Ocelic, N.; Hillenbrand, R. Infrared-Spectroscopic Nanoimaging with a Thermal Source. *Nat. Mater.* **2011**, *10* (5), 352–356. https://doi.org/10.1038/nmat3006.

[52] Felts, J. R.; Kjoller, K.; Lo, M.; Prater, C. B.; King, W. P. Nanometer-Scale Infrared Spectroscopy of Heterogeneous Polymer Nanostructures Fabricated by Tip-Based Nanofabrication. *ACS Nano* **2012**, *6* (9), 8015–8021. https://doi.org/10.1021/nn302620f

[53] Yeo, B.-S.; Amstad, E.; Schmid, T.; Stadler, J.; Zenobi, R. Nanoscale Probing of a Polymer-Blend Thin Film with Tip-Enhanced Raman Spectroscopy. *Small* **2009**, *5* (8), 952–960. https://doi.org/10.1002/smll.200801101

[54] Huth, F.; Govyadinov, A.; Amarie, S.; Nuansing, W.; Keilmann, F.; Hillenbrand, R. Nano-FTIR Absorption Spectroscopy of Molecular Fingerprints at 20 nm Spatial Resolution. *Nano Lett.* **2012**, *12* (8), 3973–3978. https://doi.org/10.1021/nl301159v

[55] Ashkin, A. Acceleration and Trapping of Particles by Radiation Pressure. Phys. Rev. Lett. 1970, 24 (4), 156–159. https://doi.org/10.1103/PhysRevLett.24.156

[56] Ashkin, A.; Dziedzic, J. M.; Bjorkholm, J. E.; Chu, S. Observation of a Single-Beam Gradient Force Optical Trap for Dielectric Particles. *Opt. Lett.* **1986**, *11* (5), 288–290. https://doi.org/10.1364/OL.11.000288

[57] Jones, P. H.; Maragò, O. M.; Volpe, G. *Optical Tweezers: Principles and Applications*; Cambridge University Press, 2015

[58] Maragò, O. M.; Jones, P. H.; Gucciardi, P. G.; Volpe, G.; Ferrari, A. C. Optical Trapping and Manipulation of Nanostructures. Nat. Nanotechnol. 2013, 8 (11), 807–819. https://doi.org/10.1038/nnano.2013.208

[59] Thurn, R.; Kiefer, W. Raman-Microsampling Technique Applying Optical Levitation by Radiation Pressure. *Appl. Spectrosc.* **1984**, *38* (1), 78–83. https://doi.org/10.1366/0003702844554440

[60] Petrov, D. V. Raman Spectroscopy of Optically Trapped Particles. *J. Opt. Pure Appl. Opt.* **2007**, *9* (8), S139. https://doi.org/10.1088/1464-4258/9/8/S06

[61] Polimeno, P.; Magazzù, A.; Iatì, M. A.; Patti, F.; Saija, R.; Esposti Boschi, C. D.; Donato, M. G.; Gucciardi, P. G.; Jones, P. H.; Volpe, G.; Maragò, O. M. Optical Tweezers and Their Applications. *J. Quant. Spectrosc. Radiat. Transf.* **2018**, *218*, 131–150. https://doi.org/10.1016/j.jqsrt.2018.07.013

[62] Xie, C.; Chen, D.; Li, Y. Raman Sorting and Identification of Single Living Micro-Organisms with Optical Tweezers. *Opt. Lett.* **2005**, *30* (14), 1800–1802. https://doi.org/10.1364/OL.30.001800

[63] Lambert, P. J.; Whitman, A. G.; Dyson, O. F.; Akula, S. M. Raman Spectroscopy: The Gateway into Tomorrow's Virology. *Virol. J.* **2006**, *3* (1), 51. https://doi.org/10.1186/1743-422X-3-51

[64] Wu, M.; Ling, D.; Ling, L.; Li, W.; Li, Y. Stable Optical Trapping and Sensitive Characterization of Nanostructures Using Standing-Wave Raman Tweezers. *Sci. Rep.* **2017**, *7*, 42930. https://doi.org/10.1038/srep42930

[65] Maragó, O. M.; Bonaccorso, F.; Saija, R.; Privitera, G.; Gucciardi, P. G.; Iatì, M. A.; Calogero, G.; Jones, P. H.; Borghese, F.; Denti, P.; Nicolosi, V.; Ferrari, A. C. Brownian Motion of Graphene. *ACS Nano* **2010**, *4* (12), 7515–7523. https://doi.org/10.1021/nn1018126

[66] Svedberg, F.; Li, Z.; Xu, H.; Käll, M. Creating Hot Nanoparticle Pairs for Surface-Enhanced Raman Spectroscopy through Optical Manipulation. *Nano Lett.* **2006**, *6* (12), 2639–2641. https://doi.org/10.1021/nl062101m

[67] Patra, P. P.; Chikkaraddy, R.; Tripathi, R. P. N.; Dasgupta, A.; Kumar, G. V. P. Plasmofluidic Single-Molecule Surface-Enhanced Raman Scattering from Dynamic Assembly of Plasmonic Nanoparticles. *Nat. Commun.* **2014**, *5*, 4357. https://doi.org/10.1038/ncomms5357

[68] Fazio, B.; D'Andrea, C.; Foti, A.; Messina, E.; Irrera, A.; Donato, M. G.; Villari, V.; Micali, N.; Maragò, O. M.; Gucciardi, P. G. SERS Detection of Biomolecules at Physiological pH via Aggregation of Gold Nanorods Mediated by Optical Forces and Plasmonic Heating. *Sci. Rep.* **2016**, *6*, 26952. https://doi.org/10.1038/srep26952

[69] Foti, A.; D'Andrea, C.; Villari, V.; Micali, N.; Donato, M. G.; Fazio, B.; Maragò, O. M.; Gillibert, R.; Lamy de la Chapelle, M.; Gucciardi, P. G. Optical Aggregation of Gold Nanoparticles for SERS Detection of Proteins and Toxins in Liquid Environment: Towards Ultrasensitive and Selective Detection. *Materials* **2018**, *11* (3), 440

[70] Ajito, K.; Torimitsu, K. Single Nanoparticle Trapping Using a Raman Tweezers Microscope. *Appl. Spectrosc.* **2002**, *56* (4), 541–544

[71] Singh, B.; Sharma, N. Mechanistic Implications of Plastic Degradation. *Polym. Degrad. Stab.* **2008**, *93* (3), 561–584. https://doi.org/10.1016/j.polymdegradstab.2007.11.008.

[72] Galgani, F.; Hanke, G.; Werner, S.; De Vrees, L. Marine Litter within the European Marine Strategy Framework Directive. *ICES J. Mar. Sci.* **2013**, *70* (6), 1055–1064. https://doi.org/10.1093/icesjms/fst122.

[73] Loos, C.; Syrovets, T.; Musyanovych, A.; Mailänder, V.; Landfester, K.; Nienhaus, G. U.; Simmet, T. Functionalized Polystyrene Nanoparticles as a Platform for Studying Bio–Nano Interactions. *Beilstein J. Nanotechnol.* **2014**, *5* (1), 2403–2412. https://doi.org/10.3762/bjnano.5.250.

[74] Ghislain, L. P.; Switz, N. A.; Webb, W. W. Measurement of Small Forces Using an Optical Trap. *Rev. Sci. Instrum.* **1994**, *65* (9), 2762–2768. https://doi.org/10.1063/1.1144613.

[75] https://www.nist.gov/pml/engineering-physics-division/standard-reference-materials-engineering-physics-division

[76] Török, B.; Kulkarni, A.; DeSousa, R.; Satuluri, K.; Török, M.; Prakash, G. K. S. Synthesis and Application of Polystyrene Nanospheres Supported Platinum Catalysts in Enantioselective Hydrogenations. *Catal. Lett.* **2011**, *141* (10), 1435. https://doi.org/10.1007/s10562-011-0672-5.

[77] Ashkin, A. Forces of a Single-Beam Gradient Laser Trap on a Dielectric Sphere in the Ray Optics Regime. *Biophys. J.* **1992**, *61* (2), 569–582. https://doi.org/10.1016/S0006-3495(92)81860-X

[78] https://scientificpolymer.com/technical-library/refractive-index-of-polymers-by-index/

[79] Balakrishnan, G.; Déniel, M.; Nicolai, T.; Chassenieux, C.; Lagarde, F. Towards More Realistic Reference Microplastics and Nanoplastics: Preparation of Polyethylene Micro/Nanoparticles with Biosurfactant. *Environ. Sci. Nano* **2018**. https://doi.org/10.1039/C8EN01005F.

[80] Moncho-Jordá, A.; Martínez-López, F.; Hidalgo-Álvarez, R. The Effect of the Salt Concentration and Counterion Valence on the Aggregation of Latex Particles at the Air/Water Interface. *J. Colloid Interface Sci.* **2002**, *249* (2), 405–411. https://doi.org/10.1006/jcis.2002.8224.

[81] Nuelle, M.-T.; Dekiff, J. H.; Remy, D.; Fries, E. A New Analytical Approach for Monitoring Microplastics in Marine Sediments. *Environ. Pollut.* **2014**, *184*, 161–169. https://doi.org/10.1016/j.envpol.2013.07.027

[82] Krishnan, R. S. Raman Spectrum of Quartz. *Nature* **1945**, *155* (3937), 452–452. https://doi.org/10.1038/155452a0.

[83] Tomar, V.; Niranjan, P. Raman Spectroscopy of Algae: A Review. *J. Nanomedicine Nanotechnol.* **2012**, *03* (02). https://doi.org/10.4172/2157-7439.1000131.

[84] Casabella, S.; Scully, P.; Goddard, N.; Gardner, P. Automated Analysis of Single Cells Using Laser Tweezers Raman Spectroscopy. *Analyst* **2016**, *141* (2), 689–696. https://doi.org/10.1039/C5AN01851J

[85] Lee, K. S.; Palatinszky, M.; Pereira, F. C.; Nguyen, J.; Fernandez, V. I.; Mueller, A. J.; Menolascina, F.; Daims, H.; Berry, D.; Wagner, M.; Stocker, R. An Automated Raman-Based Platform for the Sorting of Live Cells by Functional Properties. *Nat. Microbiol.* **2019**, *4* (6), 1035. https://doi.org/10.1038/s41564-019-0394-9.

[86] Bernatová, S.; Donato, M. G.; Ježek, J.; Pilát, Z.; Samek, O.; Magazzù, A.; Maragò, O. M.; Zemánek, P.; Gucciardi, P. G. Wavelength-Dependent Optical Force Aggregation of Gold Nanorods for SERS in a Microfluidic Chip. *J. Phys. Chem. C* **2019**, *123* (9), 5608–5615. https://doi.org/10.1021/acs.jpcc.8b12493.